frontiers | Frontiers in Earth Science

TYPE Original Research
PUBLISHED 18 March 2025
DOI 10.3389/feart.2025.1548465

OPEN ACCESS

EDITED BY
Xiya Zhang,
China Meteorological Administration, China

REVIEWED BY
Chong Xu,
Ministry of Emergency Management, China
Yanyan Li,
Beijing University of Technology, China
Qingli Zeng,
University of Chinese Academy of Sciences, China

*CORRESPONDENCE
Lianji Liang,
lianglianji512@163.com
Fuchu Dai,
daifc@bjut.edu.cn

RECEIVED 19 December 2024
ACCEPTED 17 February 2025
PUBLISHED 18 March 2025

CITATION
Liang L, Dai F, Zhu Y and Pan R (2025) Preliminary investigation of hummocky landforms and hyper-mobility of the Bingda landslide, northeastern Tibetan Plateau. *Front. Earth Sci.* 13:1548465. doi: 10.3389/feart.2025.1548465

Preliminary investigation of hummocky landforms and hyper-mobility of the Bingda landslide, northeastern Tibetan Plateau

Lianji Liang[1,2]*, Fuchu Dai[1]*, Yuxuan Zhu[1] and Rongshen Pan[1]

[1]College of Architecture and Civil Engineering, Beijing University of Technology, Beijing, China, [2]State Key Laboratory of Earthquake Dynamics, Institute of Geology, China Earthquake Administration, Beijing, China

Rapid and long-runout landslides characterized by their high speed, long distance mobility, and huge capacity and volume would pose significant threats to infrastructure and life safety. In this study, a rapid and long-runout landslide that occurred in the Bingda village of the northeastern Tibetan Plateau, which was triggered by heavy rainfall in June 2017, was preliminarily investigated. On the basis of detailed field surveys, high-resolution satellite imagery analysis, and laboratory tests, the morphological and sedimentological features of the landslide were described, and the formation mechanism of hummocky landforms and its insight into the extraordinary movement of the Bingda landslide was deduced. The field investigation and satellite imagery analysis showed that there were nearly 200 hummocks, mostly with normal circular bases and with a height of ~0.1 m–7.5 m, distributed in the transfer and accumulation areas of the landslide. The height and number density of the hummocks decreased away from the transfer area to the accumulation area and displayed higher heights at the outer bends of the gully channel than that at the inner bends of it. The characteristics of the spatial distribution and the composition of hummocks indicated that significant generation and dissipation of pore-water pressure within the loose and saturated silty clay layer in the runout path was the most probable reason for the formation of hummocky landforms. This study also provided insights into the hypermobility mechanisms of the Bingda landslide, suggesting that this landslide began with the sliding failure of the weathered colluvium in the source area, and then the landslide debris traveled into the channel and impacted sudden undrained loading and rapid shearing to the underlying silty clay layers in the gully. These processes generated pore-water pressure and reduced the effective stress within the soil particles, resulting in a decrease in the frictional resistance in the substrate, finally facilitating the rapid and long-runout movement of the landslide.

KEYWORDS

rapid and long-runout, landslide, hummock, Tibetan Plateau, rainfall

1 Introduction

Rapid and long-runout landslides are characterized by their extraordinary speed, long distance mobility, and huge capacity and volume, resulting in catastrophic damage to infrastructure and posing grave threats to life safety (Heim, 1882; Legros, 2002; Hungr and Evans, 2004; Hungr et al., 2014). Extensive insights into the kinematic progression of these landslides have been derived from studies on their surface morphology and sedimentological structures (Strom, 2006; Shea and van, 2008; Iverson et al., 2015; Dufresne et al., 2016; Strom and Abdrakhmatov, 2018). The hummock is one of the most striking and common morphological features, seen as isolated or clustered mounds, either rounded or conical in form, which could characterize high-speed sliding. The hummocks have been documented in a wide spectrum of high-energy geological events, including large landslides or rock-debris avalanches (Hewitt, 1999; Linnell et al., 2011; Dai et al., 2019; Wang et al., 2019; Dufresne and Geertsema, 2019; Zeng et al., 2019; Zeng et al., 2021), volcanic edifices (Voight et al., 1981; Ui, 1983; Siebert, 1984; Andrade and van Wyk de Vries, 2010; Yoshida, 2013; 2014; Paguican et al., 2014), and glacier activities (Benn and Evans, 1998; Haeberli et al., 2004; Iturrizaga, 2012; Jermyn and Geertsema, 2015; Reznichenko et al., 2017).

A series of field investigation, laboratory experiments, and model simulations have been conducted in order to explain the formation mechanisms of hummocky landforms. Morphologic studies of hummocks have been conducted on the quantitative and semi-quantitative analyses of the relationship of the elements of hummocks, including the size, orientation, and spacing, with the flow direction of rock-debris avalanches (Yoshida and Sugai, 2010; Yoshida, 2014). Hummocky landforms may appear as blocks ranging in size from a few meters to hundreds of meters in diameter (Ui et al., 2000) or as discrete avalanche blocks interspersed in a matrix of finer materials (Glicken, 1996); the facts that have been explained to be due to the fault formation during mass spreading (Shea and van, 2008; Paguican et al., 2012) or due to basal shear and extensional regimes in the moving mass (Dufresne and Davies, 2009). Paguican et al. (2014) summarized that hummocks form along low-angle basal fault and high-angle normal faults, proposing that the morphology and spatial distribution of hummocks were attributed to the interplay of the number density of normal, thrust, and strike–slip faults (Dufresne and Geertsema, 2019). Shea and van (2008) and Paguican et al. (2012) suggested that the morphology and spatial distribution of hummocks were not only associated with the fault formation during mass spreading but was also related with the basal shear and extensional regimes in the moving mass (Dufresne and Davies, 2009). Prominent elongated, sub-parallel alignments hummocks have also been interpreted as remnants of longitudinal ridges induced by parallel strike–slip faults related to lateral velocity changes (Shea and van, 2008; Dufresne and Davies, 2009; Andrade and van Wyk de Vries, 2010). Undoubtedly, the hummocky landforms and their evolution and formation mechanisms could provide valuable insights into the kinematics and dynamics of landslides (Shea and van, 2008; Paguican et al., 2012; Paguican et al., 2014).

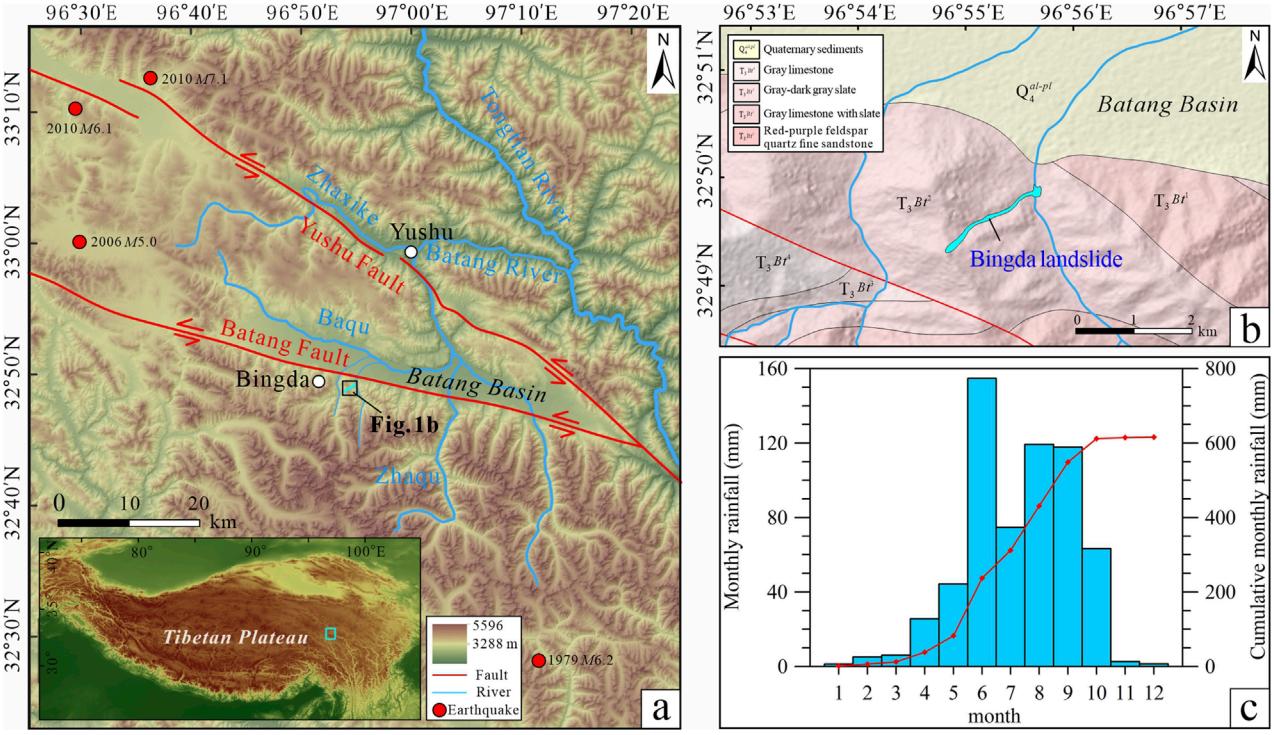

FIGURE 1
(A) Geological background of the study area and the location of the Bingda landslide. **(B)** Geologic sketch setting of the Bingda landslide. **(C)** Rainfall data of the Yushu area in 2017.

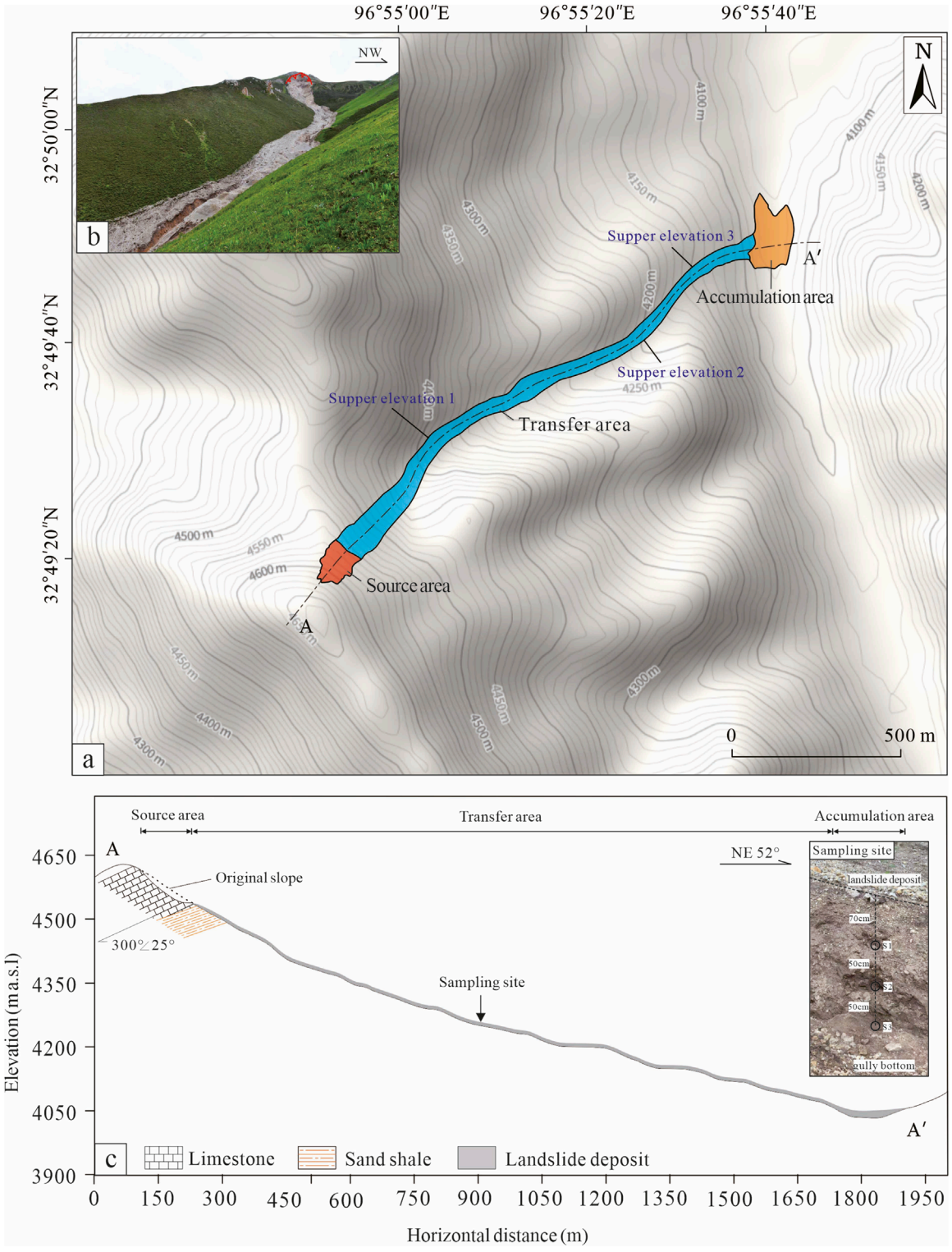

FIGURE 2
(A) Topographic contour map of the Bingda landslide. **(B)** Panorama photo of the Bingda landslide. **(C)** Longitudinal geological profile of the Bingda landslide and the sampling site of the river-cut section in the gully.

In this work, we studied a unique hummocky landform that was well-preserved in a rapid and long-runout landslide in the Bingda village of the northeastern Tibetan Plateau (Zhu et al., 2019; Pan, 2023) (Figure 1). The Bingda landslide was triggered in June 2017 by heavy rainfall, and the average velocity of the landslide mass reached approximately 24 m/s in the transfer area (Zhu et al.,

FIGURE 3
Spatial distribution of hummocks in the Bingda landslide.

2019). On the basis of the field investigation, high-resolution satellite imagery interpretation, and laboratory tests, the morphological and sedimentological features of the landslide were examined with an aim to understand the formation mechanisms of hummocks and shed light on the extraordinary movement of the Bingda landslide. This study contributed novel insights into the dynamic research of rapid and long-runout landslides.

2 Geological setting

The Bingda landslide was located at 32°49′17″N, 96°54′48″E, and 4,645 m above sea level (a.s.l.) in Yushu City in the northeastern Tibetan Plateau of China (Figure 1A). The study area is characterized by its location in the alpine zone, proximal to the Batang basin to the north. The left-lateral Yushu and Batang faults pass through this region and control the regional tectonic activities and earthquake events (Wu et al., 2014). This region mainly contains the Triassic limestone slate and feldspar quartz sandstone with limestone, which constitutes the main lithology of mountainous topography (Peng, 2013; Wu et al., 2014) (Figure 1B). The EW-trending Batang basin is infilled with Quaternary alluvial and diluvial deposits. A drainage channel of the Baqu River tributaries, which is a third-order tributary of the Tongtian River, flows through the front of the valley in the landslide area (Wu et al., 2014). The groundwater and atmospheric precipitation are the primary sources of runoff for these tributaries, contributing to the fragmentation and weathering of the bedrock. The climate of this region is the plateau continental monsoon climate, which is characterized by longer cold seasons and shorter warm seasons. The mean annual temperature fluctuates between - 4.3°C and 4.6°C, while the mean annual rainfall ranges between 419.7 mm and 542.0 mm. Rainfall data from the Yushu meteorological station between 2012 and 2017 indicate that the predominant rainfall period is from June to October, receiving over 70% of the total annual rainfall (Pan, 2023). In 2017, the annual rainfall reached 616.1 mm, with a significant surge in June, recording a monthly total of 154.7 mm over 25 rainfall days (Figure 1C).

3 Methodology

The boundary and zonation of the Bingda landslide were defined and verified utilizing 1.0-m resolution Century Space satellite imagery and were consulted by utilizing 0.3-m resolution Worldview 3 satellite imagery and high-resolution Google Earth imagery. A topographic map of the study area was generated from the Advanced Spaceborne Thermal Emission and Reflection Radiometer (ASTER) digital elevation models (DEMs) at http://www.gscloud.cn/home. Considering the study area's proximity (~20 km) to Batang airport, which is designated as a national no-fly-zone, a detailed field survey focusing on the mapping and orientation of hummocks across various scales was undertaken. Detailed photographic documentation and descriptions of the landslide deposits were recorded, employing a hammer for scale reference. In addition, three samples (named S1 to S3) were systematically collected from the river-cut section exposed in the gully to examine the fundamental physical properties. Undisturbed soil samples were extracted utilizing a ring knife with a diameter of 70 mm and a height of 52 mm. Then, analyses were performed to determine the water content, specific gravity, porosity, saturated and dry density, and grain size distribution. Grain size analysis was carried out on a Mastersizer 3000 laser particle size analyzer equipped at the Hebei Institute of Regional Geology and Mineral Resources Investigation.

4 Basic characteristics of the Bingda landslide

According to the high-resolution satellite image interpretation and topographical field investigation of the landslide, the landslide can be divided into three parts: source area, transfer area, and accumulation area (Figure 2A). The landslide presents a northeastward long and narrow channel shape (Figure 2B). The vertical distance difference (H) and horizontal distance difference (L) of the top and toe of the landslide are ~552 m and ~1,795 m, respectively, and the corresponding equivalent friction coefficient (H/L) is calculated as 0.308 < 0.33 (Heim, 1932; Scheidegger, 1973), exhibiting the rapid and long-runout mobility (Figure 2C).

4.1 Source area

The source area of the landslide presents a spoon shape, with the highest elevation of the main scarp reaching approximately 4,645 m, and the elevation of the toe of the rupture surface assessing

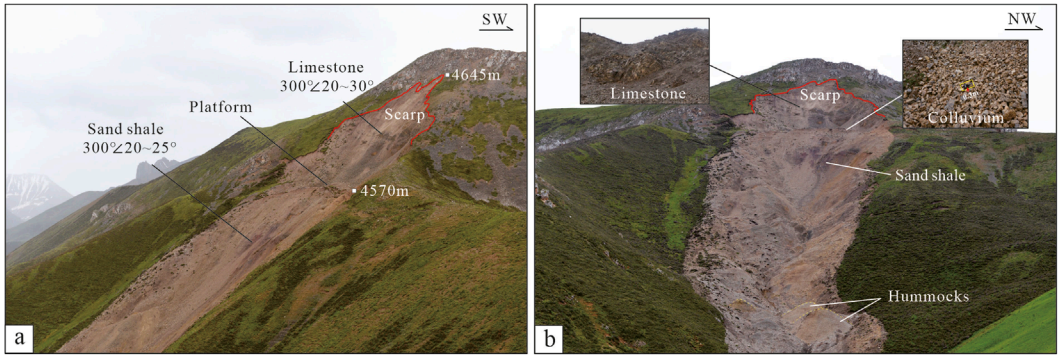

FIGURE 4
(A) Distant view of the source area of the Bingda landslide. **(B)** The front view of the source area of the Bingda landslide, and the limestone bedrock and colluvium deposits in the source area.

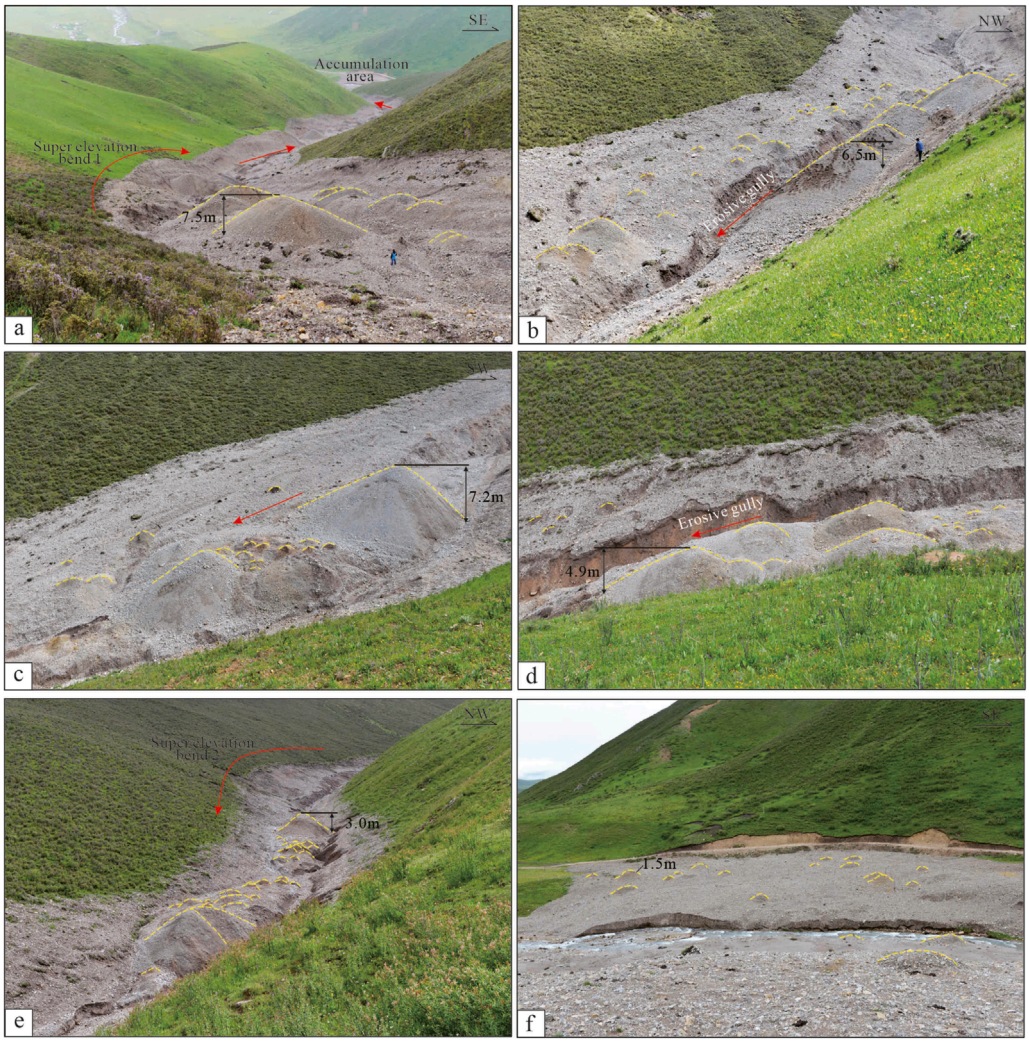

FIGURE 5
Hummocky landforms distributed in the transfer area **(A–E)** and the accumulation area **(F)** of the Bingda landslide.

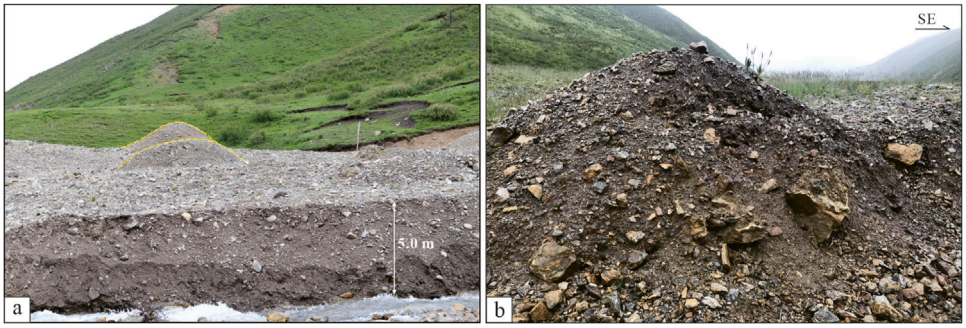

FIGURE 6
(A) Sediment profile of the accumulation area of the Bingda landslide. **(B)** Hummock distributed in the accumulation area of the Bingda landslide.

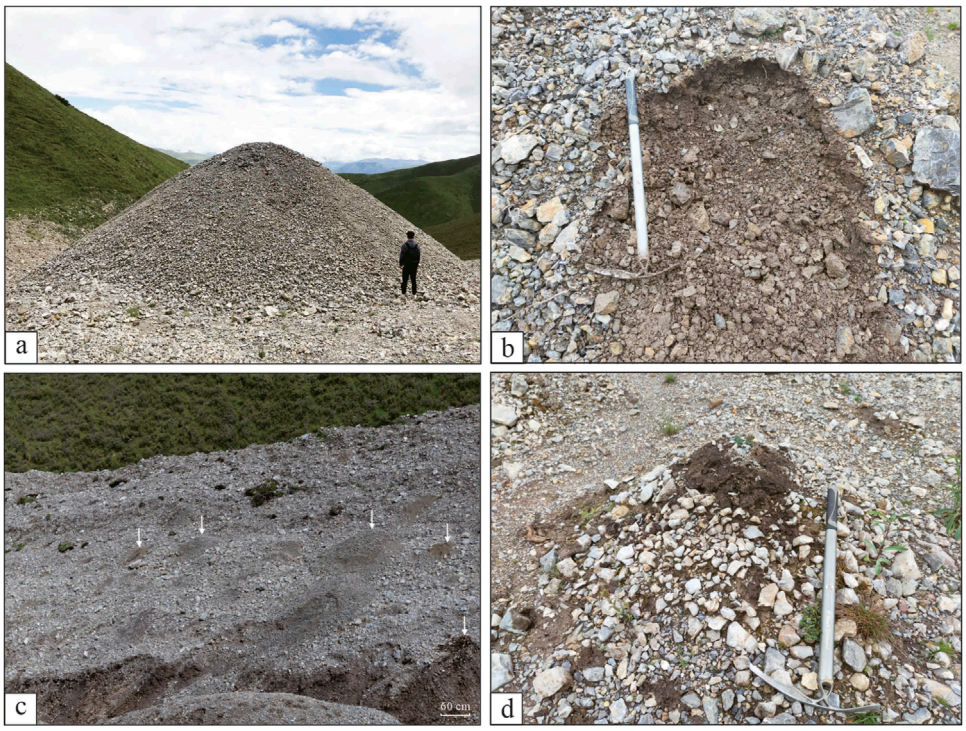

FIGURE 7
(A) Close photograph of a hummock located in the transfer area of the Bingda landslide. **(B)** Inner composition of the hummock in the transfer area. **(C, D)** Liquefaction phenomenon.

approximately 4,570 m (Figures 3, 4A). According to the remote sensing analyses and field surveys, the source area occupies ~8.8 × 10^3 m^2, and the average depth of the rupture surface was ~10 m; thus, the total volume of the main body of the landslide in the source area is approximately 8.8 × 10^4 m^3. The slope of the main scarp measures approximately 40°–50°, and the outcropping bedrock in the source area is anti-dip gray limestone with the predominant attitude of 300°<20°–30°. A platform of length ~96 m and width ~20 m was formed on the lower part of the source area, and the surface was covered by colluvium deposits mainly composed of weathered limestone fragments (Figures 3, 4B). The particle size of the colluvium deposits ranges from 0.1 m to 0.5 m, and the content of the particle size of ~0.1 m–0.3 m occupied approximately 70%. Under the platform, the anti-dip purple sand shale with the attitude of 300°<20°–25° is exposed, and it left distinct scrape marks on the surface of the bedrock. The slope structures with the upper limestone and lower sandy shale controlled the favorable conditions for the differential weathering and the deformation and failure of the slope.

4.2 Transfer area

The transfer area exhibits a long and narrow shape, with the length of ~1,557 m along the sliding axis and the width ranging from approximately 28 m to 100 m (Figure 3). The transfer area occupies a surface area of approximately 99.6 × 10^3 m^2, covering

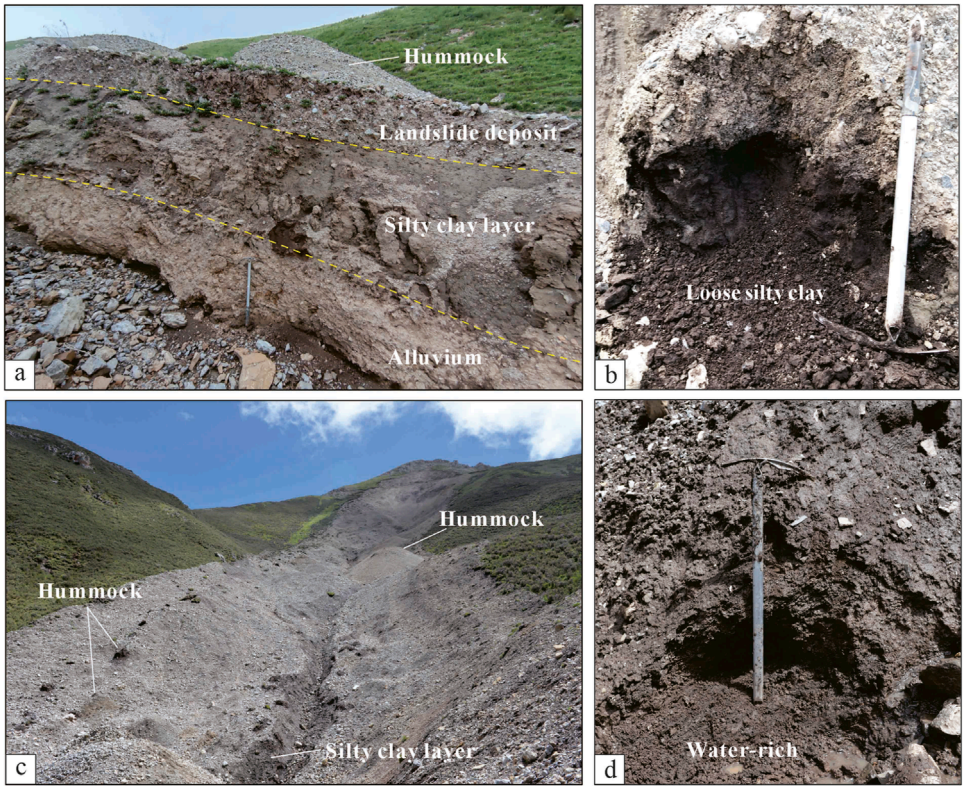

FIGURE 8
(A) Sedimentary structures of the river-cut section in the gully. **(B)** Loose structure of the black silty clay layer. **(C)** Gully profile formed by water erosion. **(D)** Water-rich and saturated silty clay layer.

TABLE 1 Results of the basic physical properties of gully samples.

Sample	d_{50} (μm)	Water (%)	ρ_w (g/cm^3)	ρ_d (g/cm^3)	G_s	e (%)
S1	11.14	20.85	1.2	1	2.62	61.98
S2	7.04	37.76	1.63	1.18	2.63	55.03
S3	7.95	20.89	1.88	1.56	2.69	42.06

over 70% of the total landslide area. The landslide mass eroded and entrained the substrate materials and the surface vegetation in the movement path, forming apparent scrape boundaries at both flanks of the landslide (Figures 5A–E). The upper part of the gully deposits were eroded and entrained by the landslide mass, amplifying the volume of the landslide mass by approximately 7.6×10^4 m^3, while most of them were accumulated in the movement path (Pan, 2023). The average slope of the transfer area is approximately 18°, transitioning from a steep slope of ~30° in the source zone to a gentler slope of ~15° in the front edge of the transfer area (Figure 2C). Due to the transformation of the channel direction, the landslide mass experienced three times the freeboard phenomenon in the curved ways of the channel during the landslide movement (Figure 2A).

4.3 Accumulation area

The accumulation area displays a fan-like shape, occupying approximately 16.8×10^3 m^2 area (Figures 3, 5F). The landslide debris that surged from the gully was hindered by the opposite mountain, causing the decrease in speed and ceasing of the debris. The accumulation area was later eroded by the river, exposing the internal sedimentary structure (Figure 6). The features of the sediment profile indicate that the upper part of the deposits primarily consists of limestone fragments, ranging in particle size from ~0.05 m to 0.5 m, while the lower part comprises silt and silty clay deposits occasionally entrained with individual limestone fragments, demonstrating an inverse grading pattern.

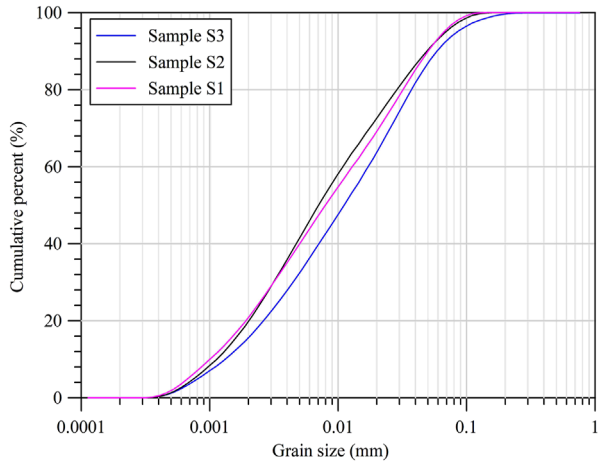

FIGURE 9
Grain size distribution of the samples collected from the gully section.

5 Morphology and sedimentology

5.1 Characteristics of hummocks

The most prominent morphological feature of the Bingda landslide is hummocky landforms, which are mainly distributed in the transfer and accumulation areas (Figures 3, 5, 6). The hummocks generally display as mounds, either individual or clustered, accounting for nearly 200 hummocks with the height of ~0.1 m–7.5 m. There are distributed 12 hummocks that are higher than 3 m, 16 with the height between ~3 m and 1 m, and approximately 171 hummocks that are less than 1 m in height. The hummocks in the transfer area exhibit higher height than those in the accumulation area, showing the decreasing trend along with the downward movement of landslide mass. In the accumulation area, the average height of the hummocks decreased significantly (Figures 3, 5F, 6). Moreover, the hummocks presented higher heights at the outer bends of the gully channel than that at the inner bends of the channel, especially at the places of super elevations (Figure 3). Most hummocks display normal circular shapes and have standard circular bases (Figure 7A), while the hummocks higher than 1 m exhibit elliptical bases due to the slope topography.

The hummocks in the transfer area were primarily covered by the gravelly and sandy limestone fragments, and the inner materials were composed of the gravel–sand fragments and black silty clay that originated from the underlying layers in the gully, which might also be affected by surficial coarseness due to the transferring of fine material by rainfall (Figure 7B). Moreover, in the transfer area, a large amount of mounds with the black silty clay sediments surrounded by limestone fragments are observed, indicating the occurrence of liquefaction in the underlying silty clay layers due to the generation of pore-water pressure (Figures 7C, D). The hummocks in the accumulation area were composed of complicated sand and silt matrices containing single, large boulders, suggesting that the entrainment of the large blocks and silty clay sediments with the landslide mass also happened in this area, influencing the distribution and composition of the hummocks.

5.2 Sedimentological structures of the landslide deposits

The sediment profile of the gully eroded by the surface water well presented the inner structures of landslide and gully deposits (Figure 8). The sedimentary profile exposed in the gully displays a thickness ranging from approximately 1.5 m to 4 m, consisting of three layers, namely, the landslide deposit, silty clay layer, and alluvial deposits from the top to the bottom (Figure 8A). The uppermost landslide deposits, averaging between about 0.2 m and 1.0 m in thickness, primarily consist of sandy and gravelly limestone fragments originating from the source area. The upper landslide fragments outcrop as a thin layer with angular centimeter-to-millimeter-sized blocks supported by a heterogeneous body composed of gravel and sandy and silty clay, presenting an inverse grading (Dufresne et al., 2016).

The black silty clay layer in the gully was distributed with a thickness ranging from approximately 0.5 m to 3 m, displaying a loose structure and water-saturated status (Figures 8B–D). The upper part of the silty clay layer was disturbed and entrained by the landslide deposits, with the entrained thickness of approximately 0.5 m–1.0 m of the silty clay layer. The bottom yellowish alluvial diluvium deposit with a high consolidation degree was exposed intermittently along the gully (Figure 8A). Table 1; Figure 9 presents the laboratory results of the basic physical properties of three samples, which were collected from the gully profile. The results indicate that the S2 sample of the silty clay layer comprises 73% of silt particles (0.005–0.075 mm). The clear trends of dry density, increasing specific gravity, and decreasing porosity from the top to the bottom in the profile are observed.

6 Discussion

6.1 Formation mechanism of hummocks

The hummocky landform is one of the most common morphological features of large landslides or rock–debris avalanches. Previous studies on the formation mechanisms of hummocks mainly focused on extensional regimes during landslide mobility (Dufresne and Davies, 2009) and faulting resulting from landslide mass spreading (Shea and van, 2008; Paguican et al., 2012). A hypothesis had also been proposed that the distribution of large boulders could act as anchors, facilitating the accumulation of debris around them, thereby forming mounds (Andrade and van Wyk de Vries, 2010). These research highlights the relationship between the features of hummock landforms and the kinematic processes of the landslides, suggesting that the perpendicular or parallel orientations of hummocky mounds are attributed to the extrusion or stretching of the landslide mass. Permafrost molards, which are conical mounds of loose debris that result from the degradation of blocks of ice rich in sediments that are mobilized by landslides (Morino et al., 2019; Beck et al., 2024), also display similar shapes with hummocky landforms. However, the hummocky landforms observed in this study exhibited a consistently uniform, round shape without any evident directivity. The composed materials of the hummocks and the inner structures of the gully profile suggested that no fault activity induced by

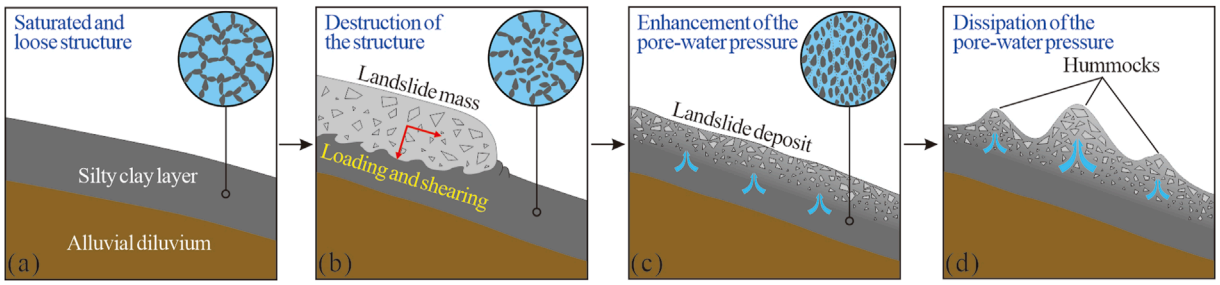

FIGURE 10
Schematic diagram of the formation processes of hummocks. **(A)** Before the landslide event, the silty clay sediments in the gully were in a saturated and loose state. **(B)** During the landslide movement, the sudden undrained loading and rapid shearing surged into the silty clay layer and resulted in the destruction of its loose structure. **(C)** The process of landslide movement induced the enhancement and concentration of the pore-water pressure within the silty clay layer. **(D)** Along with upward dissipation of the pore-water pressure, the hummocks and liquefaction phenomenon formed in the movement path of the landslide.

TABLE 2 Earthquake records in the study area in 2017 (http://data.earthquake.cn).

Date	M	Coordinates	Depth/km
2017/05/06	3.1	32.92°N, 97.18°E	11
2017/05/08	3.3	32.60°N, 97.45°E	9
2017/11/01	3.0	33.38°N, 96.16°E	10
2017/11/01	3.9	33.35°N, 96.18°E	10

the dynamic extension in the landslide mobility had occurred in this area (Paguican et al., 2014). Moreover, the Bingda landslide occurred in June, which was the rainy and high-temperature period in this region, so permafrost molards seem not to have been formed in this case. We supposed that the formation of hummocks in the Bingda landslide is mostly associated with the generation of pore-water pressure, and the loose and saturated silty clay sediments distributed in the movement path played an important role in this process.

During the landslide movement, the saturated and loose silty clay layer in the gully suffered great impact forces from the landslide mass (Figure 10A). The sudden undrained loading and rapid shearing surged into the silty clay layer in the runout path and resulted in the destruction of its loose structures (Figure 10B). This process induced a rapid enhancement and concentration of the pore-water pressure within the substrate and silty clay layer, causing the reduction of the effective stress of soil particles and the shear stress in the basal layer (Figure 10C). This could also be supported by the theoretical model that the high motion of the landslide would contribute to the generation of excess pore-water pressure along the sliding surface and the saturated layer in the movement path (Sassa, 1988). The low permeability of the silty clay layer also promoted the congregation of the pore-water pressure and hindered the timely dissipation of pore-water pressure. Along with the deceleration and stabilization of landslide debris, the pore-water pressure had gradually dissipated through the underlying deposits, forming different scales of hummocks and the liquefaction phenomenon in the movement path (Figures 10D, 7C, D). The morphological features of the hummocks indicated that the height and density of hummocks are likely influenced by factors including, among others, the overlying stress of landslide deposits, movement rate of landslide mass, and the properties of the silty clay layer. The spatial distribution features of hummocks indicated that the stronger loading, higher speed, looser structure, and finer particles of the underlying sediments could benefit the generation of pore-water pressure and the formation of hummocks.

6.2 Insights into the hypermobility of the Bingda landslide

In this study area, the intense tectonic activities and long-term weathering resulted in the steepening of the slope and the formation of a mountainous-valley terrain (Figure 1), which provided a favorable geological background for weakening the bedrock of the slope in strength and the occurrence of landslide hazards. According to the field investigation, the bedrock mainly exposed in the upper part of the source area is anti-dip limestone, and the lower part is anti-dip sand shale (Figure 4). Owing to the gravity forcing and weathering, limestone gradually reduced in strength and fractured intensely, forming thick colluvium deposits in the source area, of which the weathering processes have also been accelerated by the peri-glacial environment and the action of frost weathering in this region. These basic conditions have controlled the deformation and failure of the debris mass slopes in the source area.

According to the regional meteorological and historical earthquake records in this period, this region has experienced overall continuous 25 rainfall days in June 2017 (Figure 1C), but there were no earthquake events recorded (Table 2). Although this region has suffered long-term intense tectonic activities and strong earthquakes, which could affect the fracture development of bedrocks, the earthquake trigger for the Bingda landslide could be excluded. The heavy rainfall increased the high-level groundwater and surface runoff in this region, inducing the stagnation of water at the bottom of the source area and the saturation in the silty clay layers in the transfer and accumulation areas. The Bingda landslide

started from the sliding failure of the colluviums in the steep slope and sheared out from the interface of the limestone and sand shale bedrock. The landslide mass then traveled into the transfer area and entrained the loose silty clay in the runout path and the surface water present in the channel. In this process, the silty clay sediments became subject to sudden undrained loading and rapid shearing, and the substrate underwent a significant increase in pore-water pressure (Sassa, 1985; Hungr et al., 2014) and the reduction of effective stress within the soil particles and frictional resistance in the substrate (Hutchinson and Bhandari, 1971; Wang et al., 2002; Hungr and Evans, 2004; Sassa and Wang, 2005), facilitating the rapid and long-runout mobility of the Bingda landslide.

7 Conclusion

In June 2017, the heavy rainfall triggered a rapid and long-runout landslide with the vertical distance difference of ~552 m, the horizontal distance of ~1,795 m, and an estimated volume of 8.8×10^4 m^3. In the landslide area, we observed the striking hummocky landforms, accounting for nearly 200 hummocks, with the height ranging from ~7.5 m to 0.1 m. The spatial distribution and sedimentary features of hummocks suggested that the formation mechanisms of the hummocks could be attributed to the generation and dissipation processes of pore-water pressure in the saturated and loose silty clay layers in the movement path. This study also generalized that the landslide began with the sliding failure of the weathered colluvium from the steep slope and traveled into the gully channel. In these processes, the silty clay sediments suffered the sudden undrained loading and rapid shearing of the upper landslide mass, causing the generation and concentration of pore-water pressure, and the reduction of the frictional resistance in the substrate, resulting in the rapid and long-runout movement of the Bingda landslide.

Data availability statement

The original contributions presented in the study are included in the article/supplementary material; further inquiries can be directed to the corresponding authors.

Author contributions

LL: conceptualization, data curation, formal analysis, funding acquisition, investigation, methodology, project administration, writing–original draft, and writing–review and editing. FD: conceptualization, investigation, methodology, writing–review and editing, and funding acquisition. YZ: data curation, investigation, and writing–original draft. RP: investigation and writing–original draft.

Funding

The author(s) declare that financial support was received for the research, authorship, and/or publication of this article. This work was supported by the second comprehensive scientific expedition project of the Qinghai–Tibet Plateau (2019QZKK0905-05) and the Open Fund of the State Key Laboratory of Earthquake Dynamics (LED2023B03).

Acknowledgments

The authors express their sincere appreciation to the editor and reviewers for providing insightful and valuable suggestions and improvements to the manuscript.

Conflict of interest

The authors declare that the research was conducted in the absence of any commercial or financial relationships that could be construed as a potential conflict of interest.

The reviewer YL declared a shared affiliation with the authors to the handling editor at time of review.

Generative AI statement

The author(s) declare that no generative AI was used in the creation of this manuscript.

Publisher's note

References

Andrade, S., and van Wyk de Vries, B. (2010). Structural analysis of the early stages of catastrophic stratovolcano flank-collapse using analogue models. *Bull. Volcanol.* 72, 771–789. doi:10.1007/s00445-010-0363-x

Beck, C., Font, M., Conway, S. J., Philippe, M., Clément, J., and Morino, C. (2024). Mountain permafrost landslides: experimental study investigating molard formation processes. *Geomorphology* 461, 109317. doi:10.1016/j.geomorph.2024.109317

Benn, D. I., and Evans, D. J. A. (1998). *Glaciers and glaciation*. London: Arnold, 734.

Dai, Z. L., Wang, F. W., Cheng, Q. G., Wang, Y. F., Yang, H. F., Lin, Q. W., et al. (2019). A giant historical landslide on the eastern margin of the Tibetan Plateau. *Bull. Eng. Geol. Environ.* 78 (3), 2055–2068. doi:10.1007/s10064-017-1226-x

Dufresne, A., Bosmeier, A., and Prager, C. (2016). Sedimentology of rock avalanche deposits-case study and review. *Earth Sci. Rev.* 163, 234–259. doi:10.1016/j.earscirev.2016.10.002

Dufresne, A., and Davies, T. R. H. (2009). Longitudinal ridges in mass movement deposits. *Geomorphology* 105 (3-4), 171–181. doi:10.1016/j.geomorph.2008.09.009

Dufresne, A., and Geertsema, M. (2019). Rock slide–debris avalanches: flow transformation and hummock formation, examples from British Columbia. *Landslides* 17, 15–32. doi:10.1007/s10346-019-01280-x

Glicken, H. (1996). *Rockslide-debris avalanche of may 18, 1980, mount st. Helens volcano*, 96-677. Washington: USGS Open-file Report, 1–90.

Haeberli, W., Huggel, C., Kääb, A., Oswald, S., Polkvoj, A., Zotikov, I., et al. (2004). The Kolka-Karmadon rock/ice slide of 20 September 2002-an extraordinary event of historical dimensions in North Ossetia (Russian Caucasus). *J. Glaciol.* 50, 533–546. doi:10.3189/172756504781829710

Heim, A. (1882). Der Bergsturz von Elm. *Z. Der Dtsch. Geol. Ges.* 34, 74–115.

Heim, A. (1932). "Landslides and human lives (bergsturz and menschenleben)," in *Bi-tech publishers*. Editor N. Skermer (Vancouver, BC), 196.

Hewitt, K. (1999). Quaternary moraines vs catastrophic rock avalanches in the Karakoram Himalaya, Northern Pakistan. *Quat. Res.* 51, 220–237. doi:10.1006/qres.1999.2033

Hungr, O., and Evans, S. G. (2004). Entrainment of debris in rock avalanches: an analysis of a long runout mechanism. *Geol. Soc. Am. Bull.* 116 (9-10), 1240–1252. doi:10.1130/b25362.1

Hungr, O., Leroueil, S., and Picarelli, L. (2014). The Varnes classification of landslide types, an update. *Landslides* 11, 167–194. doi:10.1007/s10346-013-0436-y

Hutchinson, J. N., and Bhandari, R. K. (1971). Undrained loading, A fundamental mechanism of mudflows and other mass movements. *Géotechnique* 21 (4), 353–358. doi:10.1680/geot.1971.21.4.353

Iturrizaga, L. (2012). Hummocky debris landforms in the Chapursan Valley (Karakoram range, Pakistan): a glacio-geomorphological investigation. *Geomorphology* 169-170, 1–16. doi:10.1016/j.geomorph.2011.10.023

Iverson, R. M., George, D. L., Allstadt, K., Reid, M. E., Collins, B. D., Vallance, J. W., et al. (2015). Landslide mobility and hazards: implications of the 2014 Oso disaster. *Earth Planet. Sci. Lett.* 412, 197–208. doi:10.1016/j.epsl.2014.12.020

Jermyn, C., and Geertsema, M. (2015). An overview of some recent large landslide types in Nahanni National Park, Northwest Territories, Canada. Engineering geology for society and territory -volume 1: climate change and. *Eng. Geol.* 1, 315–320. doi:10.1007/978-3-319-09300-0_59

Legros, F. (2002). The mobility of long-runout landslides. *Eng. Geol.* 63, 301–331. doi:10.1016/s0013-7952(01)00090-4

Linnell, T., Brideau, M. A., and Procter, J. (2011). Contrasting the morphology and internal structure of hummocky mounds in two landslide deposits. *EGU Sess. NH3* 3.

Morino, C., Conway, S. J., Helgason, J. K., Hillier, J., Butcher, F. E., Balme, M. R., et al. (2019). Molards as an indicator of permafrost degradation and landslide process. *Earth Planet. Sci. Lett.* 516, 136–147. doi:10.1016/j.epsl.2019.03.040

Paguican, E. M. R., van, W. de V. B., and Lagmay, A. M. F. (2014). Hummocks: how they form and how they evolve in rockslide-debris avalanches. *Landslides* 11, 67–80. doi:10.1007/s10346-012-0368-y

Paguican, E. M. R., van Wyk de Vries, B., and Lagmay, A. M. F. (2012). Volcano-tectonic controls and emplacement kinematics of the Iriga debris avalanches (Philippines). *Bull. Volcanol.* 74, 2067–2081. doi:10.1007/s00445-012-0652-7

Pan, R. S. (2023). "Research on the mechanisms of a rapid and long-runout landslide," in *Yushu Bingda* (Thesis: Beijing University of Technology). (in Chinese with English Abstract).

Peng, L. (2013). *Yushu "4.14" earthquake secondary geological disasters in the development and distribution*. Beijing), Thesis: China University of Geosciences. (in Chinese with English Abstract).

Reznichenko, N. V., Andrews, G. R., Geater, R. E., and Strom, A. (2017). Multiple origins of large hummock deposits in Alai Valley, Northern Pamir: implications for palaeoclimate reconstructions. *Geomorphology* 285, 347–362. doi:10.1016/j.geomorph.2017.02.019

Sassa, K. (1985). "The mechanism of debris flows," in *Proceedings, 11th international conference on* (San Francisco: Soil Mechanics and Foundation Engineering), 1, 1173–1176.

Sassa, K. (1988). "Special lecture: geotechnical model for the motion of landslides," in *Proceedings of the 5th international symposium on landslide* (Rotterdam: A. A. Balkema), 1, 37–55.

Sassa, K., and Wang, G. H. (2005). "Mechanism of landslide-triggered debris flows: liquefaction phenomena due to the undrained loading of torrent deposits," in *Debris-flow hazards and related phenomena*, 81–104.

Scheidegger, A. E. (1973). On the prediction of the reach and velocity of catastrophic landslides. *Rock Mech. Rock Eng.* 5 (4), 231–236. doi:10.1007/bf01301796

Shea, T., and van, W. de V. B. (2008). Structural analysis and analogue modeling of the kinematics and dynamics of rockslide avalanches. *Geosphere* 4 (4), 657–686. doi:10.1130/ges00131.1

Siebert, L. (1984). Large volcanic debris avalanches: characteristics of source areas, deposits, and associated eruptions. *J. Volcanol. Geotherm. Res.* 22, 163–197. doi:10.1016/0377-0273(84)90002-7

Strom, A. (2006). "Morphology and internal structure of rockslides and rock avalanches: grounds and constraints for their modeling," in *Landslides from massive rock slope failure, NATO Sciences Series, IV. Earth and environmental Sciences*. Editor S. G. Evans 49, 305–326.

Strom, A., and Abdrakhmatov, K. (2018). *Rockslides and rock avalanches of Central Asia: distribution, morphology, and internal structure*. Elsevier, 458.

Ui, T. (1983). Volcanic dry avalanche deposits: identification and comparison with non-volcanic debris stream deposits. *J. Volcanol. Geotherm. Res.* 18, 135–150. doi:10.1016/0377-0273(83)90006-9

Ui, T., Takarada, S., and Yoshimoto, M. (2000). "Debris avalanches," in *Encyclopedia of volcanoes*. Editors H. Sigurdsson, B. F. Houghton, S. R. McNutt, H. Rymer, and J. Stix (San Diego: Academic Press), 617–626.

Voight, B., Glicken, H., Janda, R. J., and Douglas, P. M. (1981). "Catastrophic rockslide avalanche of May 18," in *The 1980 eruptions of mount st. Helens*. Editors P. W. Lipman, and D. R. Mullineaux, 347–377.

Wang, F. W., Sassa, K., and Wang, G. H. (2002). Mechanism of a long-runout landslide triggered by the August 1998 heavy rainfall in Fukushima Prefecture, Japan. *Eng. Geol.* 63, 169–185. doi:10.1016/s0013-7952(01)00080-1

Wang, Y. F., Cheng, Q. G., Shi, A. W., Yuan, Y. Q., Qiu, Y. H., and Yin, B. M. (2019). Characteristics and transport mechanism of the Nyixoi Chongco rock avalanche on the Tibetan Plateau, China. *Geomorphology* 343 (Oct.15), 92–105. doi:10.1016/j.geomorph.2019.07.002

Wu, Z. H., Zhou, C. J., Feng, H., Zhang, K. Q., Lin, J. C., Ye, P. S., et al. (2014). Active faults and earthquake around Yushu in eastern Tibetan Plateau. *Geol. Bull. China* 33 (4), 419–469. doi:10.3969/j.issn.1671-2552.2014.04.003

Yoshida, H. (2013). Decrease of size of hummocks with downstream distance in the rockslide-debris avalanche deposit at Iriga volcano, Philippines: similarities with Japanese avalanches. *Landslides* 10, 665–672. doi:10.1007/s10346-013-0414-4

Yoshida, H. (2014). Hummock alignment in Japanese volcanic debris avalanches controlled by pre-avalanche slope of depositional area. *Geomorphology* 223, 67–80. doi:10.1016/j.geomorph.2014.06.024

Yoshida, H., and Sugai, T. (2010). Quantitative examination of hummock alignment in debris avalanche deposits: zenkoji debris avalanche, Usu volcano, Japan. *Geogr. Rev. Jpn. Ser. B* 83, 64–72. doi:10.4157/geogrevjapanb.83.64

Zeng, Q. L., Wei, R. Q., Mcsaveney, M., Ma, F. S., Yuan, G. X., and Liao, L. Y. (2021). From surface morphologies to inner structures: insights into hypermobility of the Nixu rock avalanche, Southern Tibet, China. *Landslides* 18, 125–143. doi:10.1007/s10346-020-01503-6

Zeng, Q. L., Zhang, L. Q., Davies, T. R. M., Yuan, G. X., Xue, X. Y., Wei, R. Q., et al. (2019). Morphology and inner structure of Luanshibao rock avalanche in Litang, China and its implications for long-runout mechanisms. *Eng. Geol.* 260, 105216. doi:10.1016/j.enggeo.2019.105216

Zhu, Y. X., Dai, F. C., and Liang, L. J. (2019). Analysis on the formation mechanism of rapid and long runout landslides in liquefaction-type in Tibetan plateau. *Adv. Eng. Sci.* 52 (6), 10–21. (in Chinese with English Abstract). doi:10.15961/j.jsuese.202000282